ARTICLE NO. 78-406R

Fluid Evaporation and Boiling Heat Transfer in the Grooves of Thin-Film Evaporators

L. L. Vasiliev,* A. N. Abramenko,† and L. E. Kanonchik‡
Luikov Heat and Mass Transfer Institute, Minsk, USSR

This work is devoted to the experimental study of fluid evaporation and boiling heat transfer in grooved thin-film evaporators, with heating under the third-order boundary conditions. Acetone is used as the test fluid. Evaporators with triangular and rectangular grooves are tested. The finite-difference calculations show that heat removal along the groove is similar to hyperbolic. As a result, the analytical model for the evaporator is constructed, and the formulas are derived to calculate the maximum heat flux provided by triangular and rectangular grooves. The optimum value of the apex angle of the triangular constant-depth groove is predicted. The maximum heat flux provided by triangular and rectangular grooves is found experimentally. A comparison of the experimental and predicted results gives a good agreement.

Nomenclature

A = cross-sectional area of the elementary node, m^2
$A(x)$ = cross-sectional area of the fluid layer in the groove in the x section, m^2
B = length formation variable
$b(x)$ = fluid layer height in the x section, m
$C(\alpha)$ = constant for a given α
$C_1(\alpha)$ = constant for $R_{cap}(x)$ determination
$C_2(\alpha)$ = constant for $A(x)$ determination
$C_3(\alpha)$ = constant for $D_h(x)$ determination
D = diameter, m
$D_h(x)$ = hydraulic fluid flow diameter in the groove in the x section, m
d_g = groove depth, m
f = friction coefficient
$h(x)$ = conventional flat meniscus height in the x section, m
h = height, m
J = definite integral
K_P = curvature coefficient
K = evaporated fluid ratio
$K(\alpha)$ = friction coefficient for the triangular groove
$K(d)$ = friction coefficient for the rectangular groove
l = spacing between elementary nodes, m
$\dot{m}_0$ = fluid flow rate into the groove in the x_0 section, kg/s
$\dot{m}(x)$ = fluid flow rate into the groove in the x section, kg/s
M = meniscus, 1/m
N_f = fluid transport factor, W/m^2
P = pressure, N/m^2
Q = heat power, W
Q_0' = hyperbola ordinate at a point x_0, W/m
q = heat flux, W/m^2
R = radius, m
$R(x)$ = meniscus radius in the x section, m
r^* = latent heat of vaporization, J/kg
T = temperature, K
t = groove width, m
$t(x)$ = conventional fluid-layer width in the x section, m
V = volume of the fluid evaporated in the groove, m^3
$V(x)$ = volume of the fluid evaporated in the groove in the x section, m^3
x, y, z = coordinates
Π = perimeter, m
α = half-apex angle of the triangular groove, deg
α_e = heat-transfer coefficient, $W/m^2 \cdot K$
β = angle between $t(x)$ and $R(x)$, deg
γ = angle between $R(x)$ and the straight line connecting the groove edges, deg
Θ = wetting angle, deg
λ = thermal conductivity, $W/m \cdot K$
μ = viscosity, $N \cdot s/m^2$
ρ = density, kg/m^3
σ = surface tension, N/m
τ = time, s

Subscripts

h = hydraulic
f = fluid
g = groove
cap = capillary
m = mean
0 = initial
max = maximum
min = minimum
n = serial number
in = internal
lon = longitudinal
lat = lateral
wet = wetted
x = groove section
x_R = groove section where the lateral meniscus is tangential to the groove walls

Superscript

w = wall

Presented as Paper 78-406 at the Third International Heat Pipe Conference, Palo Alto, Calif., May 22-24, 1978; submitted July 19, 1978; revision received May 24, 1979.

Index category: Heat Pipes.

*Professor.
†Engineer.
‡B. Sc.

I. Introduction

EVAPORATORS with screwed grooves are widely used in modern heat pipes. A knowledge of the maximum heat flux provided by the grooves is necessary to predict the parameters of the heat pipes. The heat-transfer coefficient is also of importance, as it controls a temperature drop to ensure the heat flux.

The maximum heat flux is determined primarily by groove configuration, groove length, width, and depth; for triangular grooves, it depends on the apex angle, groove material, finishing, the evaporator orientation relative to the gravitational field, the properties of the test fluid, and the thermal boundary conditions on the external surface of the heat pipe.

Heat transfer in the grooves with heating under the second-order boundary conditions is described elsewhere.[1-3] In Ref. 2, the equation derived for mean fluid velocity calculations in the groove is used to predict the total heat flux. Experiments have shown that the longitudinal meniscus causes fluid motion in the groove.

In Ref. 1, the equation, based on equal variation of hydraulic and capillary pressures of the fluid flow in the triangular groove, is obtained to predict the maximum heat flux.

The predictions are compared with the experimental data for four heat pipes with different evaporator groove apex angles. The excess of the predicted values over the experimental ones is attributed to the limited fluid transport in the axial direction.

Using this model, Feldman[3] has improved the design formula for the triangular groove and derived a new one for the rectangular groove. He has suggested to employ the finite-difference method for calculating the heat-transfer coefficient in terms of the temperature drop over the groove wall and the fluid layer.

In Refs. 1 and 3, the analytical model is based on the lateral meniscus, assuming complete wetting. However, for incomplete wetting (at which $\Theta = 90 - \alpha$), the lateral meniscus takes a flat shape, and this model becomes senseless.

In the present work, an attempt is made to determine experimentally how heat removal is affected by the groove sizes under third-order boundary conditions.[4]

Unlike Refs. 1-3, here: 1) the heat flux is supplied to the evaporator under third-order boundary conditions; 2) the heat removal is limited by the processes in the evaportor grooves; 3) the effect of the sizes of triangular and rectangular grooves on the maximum heat removal is found experimentally.

II. Experimental Setup

The experimental setup (Fig. 1a) is composed of vessel 1 ($D_{in} = 0.45$ mm; $h = 0.65$ mm), evaporator unit 10 (Fig. 1a), test fluid feed system, condenser 3, and thermal shield 2.

The evaporator unit (Fig. 1b) consists of the grooved evaporator, liquid heat exchanger, porous arteries, and two baths for the fluid from the outlet pipes. The horizontal evaporator is 0.1 m long and 0.05 m wide. Because of the symmetry, the evaporator length can be divided into two sections, each 0.05 m long. The initial length ($x_0 = 0.01$ m) contacts the porous artery (packet of stainless-steel meshes), and the remaining ($x_{max} = 0.04$ m) has a free evaporation (boiling) surface.

Condenser 3 (Fig. 1a) is a thin-sheet copper cylinder with a coolant coil. The thermal cone-shaped shield is also provided with a coil.

The test fluid feed system consists of pool 4, container 5 sustaining the test fluid at constant pressure, rotameter 8, throttle 6, liquid heat exchanger 9, and outlet pipes 7. The test fluid from pool 4 flows to container 5, then through rotameter 8 and throttle 6 to the baths. The fluid flow rate is measured by rotameter 8 and controlled by throttle 6. Heat exchanger 9 keeps the test fluid at condensation temperature. Under the capillary forces, the fluid is supplied from the baths (Fig. 1b) through the porous arteries to the evaporator grooves where evaporation (boiling) occurs. Vapor is condensed on the surface of cylinder 3 and flows down to discharge tank 11 (Fig. 1a). Thermal shield 2 does not allow vapor condensation from above to avoid drop sedimentation on the evaporator. From thermostats 12-15 the fluid flows into heat exchangers.

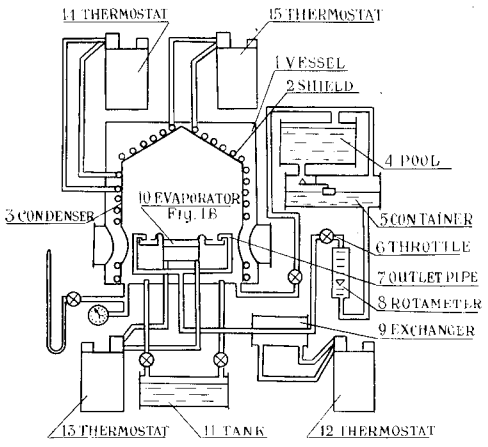

Fig. 1a Experimental setup.

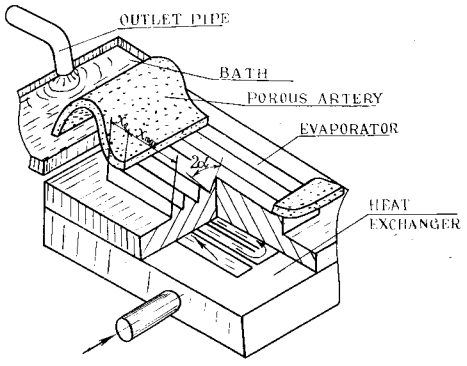

Fig. 1b Evaporator unit.

Acetone is used as the test fluid in a wide temperature range (180 + 470 K) and can wet the metal well ($\cos\theta \approx 1$).

Prior to experiment, acetone is degassed with a vacuum pump. Practically constant saturation pressure ($0.14 \cdot 10^5$ – $0.145 \cdot 10^5$ N/m^2) in the experimental setup minimizes the effect of the fluid characteristics on heat transfer.

Brass plates with triangular grooves having a different width (from $0.25 \cdot 10^{-3}$ to $0.8 \cdot 10^{-3}$ m), effective length (from $5 \cdot 10^{-3}$ to $40 \cdot 10^{-3}$ m), and apex angle (from 15 to 90 deg) and those with rectangular grooves having a different depth (from $0.2 \cdot 10^{-3}$ to $1.6 \cdot 10^{-3}$ m) are used as the extended heating surface.

III. Heat Removal along the Groove

A. Preliminary Results

In experiments, the temperature field along the groove wall is recorded. The minimum temperature is ensured at the inlet of the test fluid (section x_0). The greater the distance from the inlet, the higher the temperature observed. Its maximum value is fixed in the section $x_0 + x_{max}$ (Fig. 2). This indicates nonuniform heat transfer along the groove.

The temperature measured at the groove edges in the evaporator cross section is constant. This means that the heat removal from different evaporator grooves is also constant in this cross section.

B. Calculation of Local Heat Power

The element, whose width is equal to the groove width and whose length is half the evaporator length, is conventionally cut in the evaporator to predict a local heat power distribution along the groove. Since the groove volume is no more than 5% of the element volume, the presence of the groove on the upper edge is neglected to simplify calculations. In this case, the temperature in the element cross section is assumed to be constant.

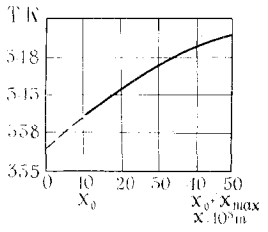

Fig. 2a Temperature distribution along the groove.

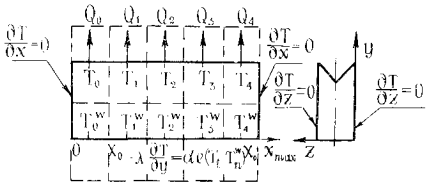

Fig. 2b Design schemes for local heat fluxes.

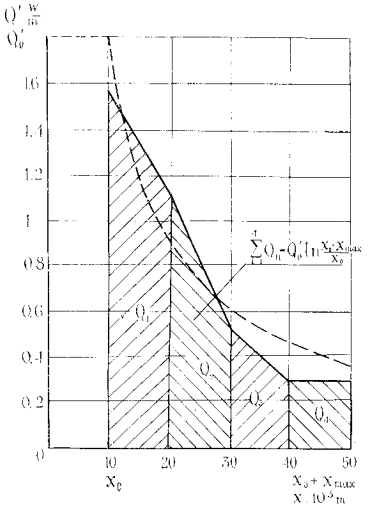

Fig. 3 Varying heat flux along the groove.

In calculations, the local heat power is subjected to the following boundary conditions:

1) Heat transfer on the lower plane of the evaporator element in contact with the liquid heat exchanger is governed by Newton-Richman's law:

$$-\lambda \frac{\partial T(x,y)}{\partial y}\bigg|_{y=0} = \alpha_e (T_f - T_n^w) \tag{1}$$

2) Temperature field on the upper plane of the evaporator element is assigned by the graphical function $T(x) = f(x)$ (Fig. 2a).

3) There is no heat removal from the face ends and side walls of the evaporator element.

Then, the chosen element is divided into the nodes, and the heat balance is written for each node. For the lower element plane, the heat balance is:

$$\alpha_e (T_f - T_n^w) A_1 + \lambda \frac{A_2}{l_1} (T_{n-1}^w - T_n^w) + \lambda \frac{A_2}{l_1} (T_{n+1}^w - T_n^w) \lambda \frac{A_1}{l_2} (T_n - T_n^w) = 0 \tag{2}$$

and for the upper-evaporator plane it is defined as:

$$\lambda \frac{A_2}{l_1} (T_{n-1} - T_n) + \lambda \frac{A_2}{l_1} (T_{n+1} - T_n) + \lambda \frac{A_1}{l_2} (T_n^w - T_n) - Q_n = 0 \tag{3}$$

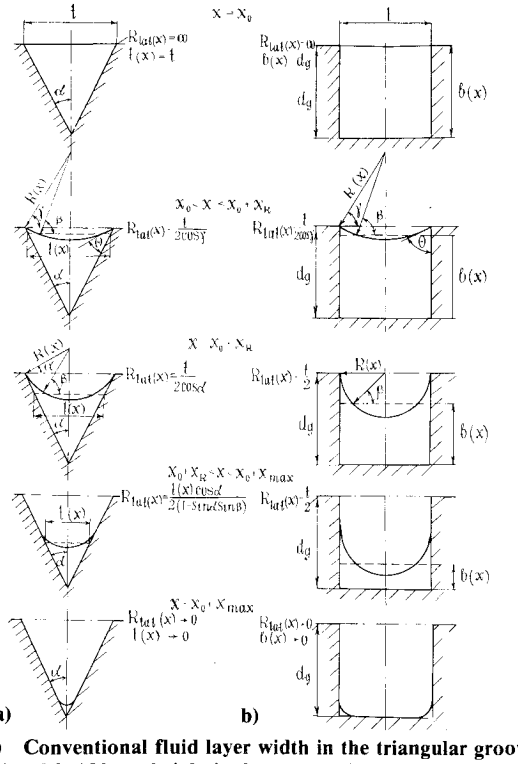

Fig. 4a) Conventional fluid layer width in the triangular groove; b) conventional fluid layer height in the rectangular groove.

In calculations, an assumption is made that the heat-transfer coefficient, the evaporator temperature in its cross section, and the coolant temperature in the liquid heat exchanger are constant.

The calculation results are given in Fig. 3. The value of tetragon areas multiplied by the scaling factor is equal to the effective heat power dissipated by the groove over the length x_{max}. The heat-power distribution along the groove can be governed by the hyperbolic function with a satisfactory accuracy up to 30%. In this case, the total heat power is determined by the area limited by this hyperbola, straight lines $X = x_0$ and $X = x_0 + x_{max}$ and by the x axis:

$$Q = \int_{x_0}^{x_0 + x_{max}} Q'_0 \frac{x_0}{x} dx = Q'_0 x_0 \ln \frac{x_0 + x_{max}}{x_0} \tag{4}$$

Dividing both sides of Eq. (4) by the value of latent vaporization heat gives the fluid flow rate into the x_0 section of the groove:

$$\dot{m} = \frac{Q'_0}{r^*} x_0 \ln \frac{x_0 + x_{max}}{x_0} \tag{5}$$

IV. Design Formulas for Maximum Heat Flux

A. Fluid Film Sizes in the Groove

Based on experimental results, Bressler[2] has concluded that the lateral meniscus caused fluid motion in the groove. This premise is used in our analytical model. For calculating convenience, the lateral meniscus arc is conventionally replaced by a straight line, namely, by the so-called conventional width $t(x)$, i.e., the cross section of the fluid layer is considered, which might be the case for a flat meniscus (Fig. 4).

Triangular Groove

The volume of the groove free of the fluid should be known to find the conventional fluid-layer thickness $t(x)$. When the artery transports a greater amount of fluid to the groove than

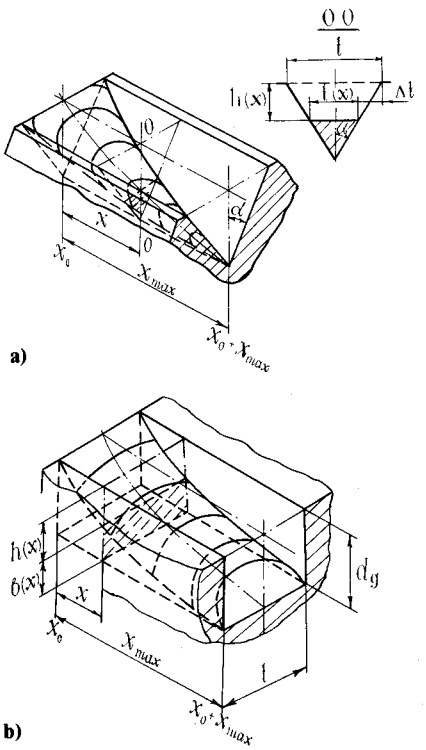

Fig. 5 Fluid flow in grooves (computer model): a) triangular groove; b) rectangular groove.

it can evaporate, the conventional fluid layer width may be assumed to coincide with the true one[2,3] (Fig. 5a)

$$t(x)_{\max}\,|_{X=x_0}=t$$

If the maximum heat flux is removed, we then have

$$t(x)_{\min}\,|_{X=x_0+x_{\max}}=0$$

For hyperbolic heat removal, the maximum volume of the fluid evaporated over the length from x_0 to $x_0+x_{\max}$ (Fig. 5a) is:

$$V_{\max}=\frac{Q_0' x_0 \tau}{r^* \rho_f}\left[\ell n\,\frac{x_0+x_{\max}}{x_0}+\sum_{i=1}^{m}(m-i)\,\ell n\,\frac{x_0+x_i}{x_0+x_{i-1}}\right] \tag{6}$$

On the other hand, this volume is equal to

$$V_{\max}=K_p t^2 ctg\alpha x_{\max} \tag{7}$$

The volume of the fluid evaporated over the length from x_0 to x_0+x is:

$$V(x)=\frac{Q_0' x_0 \tau}{r^* \rho_f}\left[\ell n\,\frac{x_0+x}{x_0}+\sum_{i=1}^{k}(k-i)\,\ell n\,\frac{x_0+x_i}{x_0+x_{i-1}}\right] \tag{8}$$

This volume is:

$$V(x)=K_p(t-2\Delta t)^2 ctg\alpha\cdot x \tag{9}$$

Equating Eqs. (6-9) and dividing them term by term gives:

$$\Delta t=\frac{t}{2}-\frac{t}{2}\left\{\frac{x_{\max}}{x}\left[\frac{\ell n\frac{x_0+x}{x_0}+\sum_{i=1}^{k}(k-i)\ell n\frac{x_0-x_i}{x_0+x_{i-1}}}{\ell n\frac{x_0+x_{\max}}{x_0}+\sum_{i=1}^{m}(m-i)\ell n\frac{x_0+x_i}{x_0+x_{i-1}}}\right]\right\}^{1/2} \tag{10}$$

The conventional width of the fluid layer within the x_0+x section is:

$$t(x)=t\left\{\frac{x_{\max}}{x}\left[\frac{\ell n\frac{x_0+x}{x_0}+\sum_{i=1}^{k}(k-i)\ell n\frac{x_0+x_i}{x_0+x_{i-1}}}{\ell n\frac{x_0+x_{\max}}{x_0}+\sum_{i=1}^{m}(m-i)\ell n\frac{x_0+x_i}{x_0+x_{i-1}}}\right]\right\}^{1/2} \tag{11}$$

As has been already mentioned, when the artery transports a greater amount of fluid to the groove than it can evaporate, the lateral meniscus in the x_0 section can be considered flat (Fig. 4). With increasing distance from this section the meniscus undergoes curvature until it becomes tangential to the groove wall near its edges with complete wetting (section x_0+x_R). The radius of this meniscus is equal to

$$R_{\text{lat}}(x_R)=\frac{t}{2\cos\alpha} \tag{12}$$

The conventional width of the fluid layer in the x_0+x_R section is:

$$t(x)=t\left[\frac{1-\sin\alpha\sin\beta(x)}{\cos^2\alpha}\right] \tag{13}$$

The angle β is found from:

$$\frac{tg\alpha}{\cos^2\alpha}\sin^2\beta(x)-2\frac{\sin\beta(x)}{\cos^3\alpha}+\frac{1}{\cos^2\alpha}\left(\frac{\pi}{2}-\alpha\right)+tg\alpha+tg^3\alpha=0 \tag{14}$$

Simultaneous solution of Eqs. (11) and (13) yields x_R.

The radius of the lateral meniscus over the length from x_0 to x_0+x_R is equal to:

$$R_{\text{lat}}(x)=\frac{t}{2\cos\gamma(x)} \tag{15}$$

The value of the angle $\gamma(x)$ is determined from:

$$t(x)=t\left[1-\frac{\sin\beta(x)\sin\alpha-\sin\gamma(x)\sin\alpha}{\cos\alpha\cos\gamma(x)}\right] \tag{16}$$

$$\frac{tg\alpha}{\cos^2\gamma(x)}\sin^2\beta(x)+tg\gamma(x)+\frac{1}{\cos^2\gamma(x)}\left[\frac{\pi}{2}-\gamma(x)\right]-2\sin\beta(x)\left[\frac{\cos\gamma(x)ctg\alpha+\sin\gamma(x)}{\cos^2\gamma(x)ctg\alpha}\right]+\frac{tg^2\gamma(x)}{ctg\alpha}=0 \tag{17}$$

The value of the wetting angle over the length from x_0 to x_0+x_R is:

$$\theta(x)=\alpha-\gamma(x) \tag{18}$$

With complete wetting within x_0+x_R through $x_0+x_{\max}$, the arc of the lateral meniscus is tangential to the groove wall. Its radius is defined as:

$$R_{\text{lat}}(x)=\frac{t(x)\cos\alpha}{2[1-\sin\alpha\sin\beta(x)]} \tag{19}$$

The value of the longitudinal meniscus in any groove section[2] is equal to:

$$R_{\text{lon}}(x)=\frac{A(x)}{\Pi_{\text{wet}}-t(x)} \tag{20}$$

$$R_{\text{lon}}(x) = \frac{t(x)\cos\alpha}{2(1-\sin\alpha)\cos\theta} = \frac{t(x)C_1(\alpha)}{\cos\theta} \tag{21}$$

In case of maximum heat removal, $R_{\text{lon}}(x)$ varies from $t \cdot C_1(\alpha)$ in the x_0 section to the value tending to zero in the $x_0 + x_{\max}$ section. As this variation of the fluid layer width always results in the required capillary pressure drop, the wetting angle of the walls due to the longitudinal meniscus is considered constant ($\theta = \text{const}$).

The cross-sectional area of the fluid flow in the section $x_0 + x$ of the groove (Fig. 5a) is:

$$A(x) = t^2(x)\frac{ctg\alpha}{4} = t^2(x)C_2(\alpha) \tag{22}$$

The hydraulic diameter is equal to:

$$D_h = 4A(x)/\Pi(x) \tag{23}$$

$$D_h = t(x)\frac{\cos\alpha}{(1+\sin\alpha)} = t(x)C_3(\alpha) \tag{24}$$

Rectangular Groove

In the rectangular groove, the conventional width of the fluid layer is the same as the groove width, i.e., $t(x) = t$. The distance from the groove edge to the conventional fluid layer width in the $x_0 + x$ section is found to be similar to $t(x)$ for the triangular groove (Fig. 5b)

$$h(x) = d \cdot \frac{x_{\max}}{x}\left[\frac{\ln\frac{x_0+x}{x_0} + \sum_{i=1}^{k}(k-i)\ln\frac{x_0+x_i}{x_0+x_{i-1}}}{\ln\frac{x_0+x_{\max}}{x_0} + \sum_{i=1}^{m}(m-i)\frac{x_0+x_i}{x_0+x_{i-1}}}\right] \tag{25}$$

For complete wetting from x_0 to $x_0 + x_R$, the lateral meniscus radius ranges from ∞ to $t/2$. The value of $h(x)$ within this length can be determined from:

$$h(x) = \frac{t}{2\cos\gamma(x)}[\sin\beta(x) - \sin\gamma(x)] \tag{26}$$

where the angle $\gamma(x)$ is defined as:

$$[\sin\beta(x) - \sin\gamma(x)]\cos\gamma(x) - [(\pi/2) - \gamma(x)] + \cos\gamma(x)\sin\gamma(x) = 0 \tag{27}$$

In the $x_0 + x_R$ section ($\gamma = 0$; $\beta = 45$ deg), we have

$$h(x) = 0.353t \tag{28}$$

Substitution of this value into Eq. (25) yields x_R. The longitudinal meniscus radius is:

$$R_{\text{lon}}(x) = t/2\cos\theta \tag{29}$$

The required capillary pressure is seen to be attained only due to varying wetting angle. Assuming that

$$\Theta|_{X=x_0} = 90 \text{ deg}$$

$$\Theta|_{X=x_0+x_{\max}} = 0 \text{ deg}$$

then

$$R_{\text{lon}}(x)|_{X=x_0} = \infty$$

$$R_{\text{lon}}(x)|_{X=x_0+x_{\max}} = t/2$$

The cross-sectional area of the fluid flow in the $x_0 + x$ section (Fig. 5b) is equal to:

$$A(x) = tb(x) \tag{30}$$

The hydraulic diameter is

$$D_h(x) = 2tb(x)/[t + b(x)] \tag{31}$$

where

$$b(x) = d - \frac{d \cdot x_{\max}}{x}\left[\frac{\ln\frac{x_0+x}{x_0} + \sum_{i=1}^{k}(k-i)\ln\frac{x_0+x_i}{x_0+x_{i-1}}}{\ln\frac{x_0+x_{\max}}{x_0} + \sum_{i=1}^{m}(m-i)\ln\frac{x_0+x_i}{x_0+x_{i-1}}}\right] \tag{32}$$

B. Analytical Model for the Evaporator

The evaporator model is based on the followin assumptions:

1) Grooves are of regular geometry.
2) The fluid flow in grooves is caused only by the surface tension forces.
3) Capillary pressure in the groove is determined by the meniscus difference in the longitudinal direction.
4) Test fluid almost completely wets the groove material.
5) Lateral meniscus is replaced by the conventional width of the fluid layer.
6) In the triangular groove, with maximum heat removal the conventional fluid layer width in the initial section is equal to the groove width, while it tends to zero in the final section.
7) In the rectangular groove, with maximum heat removal the longitudinal meniscus in the initial section is flat and is half the groove width in the final section.
8) Heat removal along the groove is hyperbolic.
9) Vapor pressure above the fluid is constant.
10) Heat transfer between the dry evaporator walls and vapor is absent.
11) Fluid flow is laminar.
12) In any section of the fluid flow the capillary pressure variation is equal to the hydraulic friction increment.

C. Design Formula for Maximum Heat Flux

Triangular Groove (Constant Groove Width)

The formula is derived assuming equal variation of the capillary pressure and hydraulic friction in any section of the fluid flow in the groove:

$$\frac{dP_{\text{cap}}}{dx} = -\frac{dP_h}{dx} \tag{33}$$

Capillary pressure in the triangular groove is:

$$dP_{\text{cap}} = \sigma dM = -\sigma\cos\Theta\frac{dR_{\text{cap}}(x)}{R^2_{\text{cap}}(x)} = -\frac{\sigma\cos\Theta}{t^2(x)C_1(\alpha)}dt \tag{34}$$

Following Hagen-Poiseuille's law, the hydraulic friction varies as:

$$dP_h = \frac{f\dot{m}(x)\mu_f}{A(x)D_h^2(x)\rho_f}dx \tag{35}$$

The fluid flow rate into any groove section can be expressed as the difference between flow rates of the whole amount of the evaporated fluid and that evaporated over the length from $X = x_0$ to $X = x_0 + x$:

$$\dot{m}(x) = \frac{Q_0'}{r^*}x_0\ln\frac{x_0+x_{\max}}{x_0+x} \tag{36}$$

At the same time

$$\frac{Q_0'}{r^*}x_0 \ell n\frac{x_0+x_{\max}}{x_0}=\frac{q_{\max}x_{\max}t}{r^*} \tag{37}$$

Then, the hydraulic friction along the groove varies as:

$$dP_h=\frac{q_{\max}x_{\max}tf\mu_f \ell n\dfrac{x_0+x_{\max}}{x_0+x}}{r^*\rho_f t^4(x)C_2(\alpha)C_3^2(\alpha)\ell n\dfrac{x_0+x_{\max}}{x_0}}dx \tag{38}$$

Equating and integrating Eqs. (34) and (38) yield:

$$\frac{\sigma\cos\Theta}{C_1(\alpha)}\int_0^t t^2(x)dt=\frac{q_{\max}tf\mu_f}{r^*\rho_f C_2(\alpha)C_3^2(\alpha)}\int_0^{x_{\max}}\frac{\ell n\dfrac{x_0+x_{\max}}{x_0+x}}{\ell n\dfrac{x_0+x_{\max}}{x_0}}dx \tag{39}$$

Upon integration we have:

$$q_{\max}=\frac{t^2r^*\rho_f\sigma\cos\Theta C_3^2(\alpha)C_2(\alpha)}{3fC_1(\alpha)\mu_f x_{\max}\left\{\dfrac{(x_0+x_{\max})}{\ell n[(x_0+x_{\max})/x_0]}-x_0\right\}} \tag{40}$$

As for this groove shape the value of the friction coefficient depends mainly on α, the following coefficient is introduced:

$$K(\alpha)=1/3f \tag{41}$$

In addition, designate

$$N_f=r^*\rho_f\sigma/\mu_f \tag{42}$$

$$C(\alpha)=C_3^2(\alpha)C_2(\alpha)/C_1(\alpha) \tag{43}$$

Finally, Eq. (40) takes the form:

$$q_{\max}=\frac{t^2N_f\cos\Theta C(\alpha)K(\alpha)}{x_{\max}\left\{\dfrac{(x_0+x_{\max})}{\ell n[(x_0+x_{\max})/x_0]}-x_0\right\}} \tag{44}$$

Triangular Groove (Constant Groove Depth)

In this case, the optimum value of the angle α is predicted, at which $q_{\max}$ is maximized.

At $d_g=\text{const}$, Eq. (44) is written as:

$$q_{\max}=\frac{d_g^2N_f\cos\Theta(1-\sin\alpha)\sin\alpha K(\alpha)}{x_{\max}\left\{\dfrac{(x_0+x_{\max})}{\ell n[(x_0+x_{\max})/x_0]}-x_0\right\}(1+\sin\alpha)^2} \tag{45}$$

The function $q_{\max}=f(\alpha)$ has a maximum at the point $\alpha=19$ deg ($2\alpha=38$ deg).

Rectangular Groove

As in the previous case, the design formula is derived assuming equal variation of the capillary pressure and hydraulic friction:

$$dP_{\text{cap}}=\sigma d\left(\frac{2\cos\Theta}{t}\right)=-\frac{2\sigma}{t}\sin\Theta d\Theta \tag{46}$$

$$P_{\text{cap}}=-\frac{2\sigma}{t}\int_{\Theta=0\,\text{deg}}^{\Theta=90\,\text{deg}}\sin\Theta d\Theta=\frac{2\sigma}{t} \tag{47}$$

$$P_h=\frac{fq_{\max}x_{\max}\mu_f}{4t^2\rho_f r^*}\int_0^{x_{\max}}\frac{[t+b(x)]^2\ell n\dfrac{x_0+x_{\max}}{x_0+x}}{b^3(x)\ell n\dfrac{x_0+x_{\max}}{x_0}}dx \tag{48}$$

In the general case, the expression for the maximum heat flux is of the form:

$$q_{\max}=-\frac{tN_fK(d)}{x_{\max}J}(\cos\Theta_{x_0+x_{\max}}-\cos\Theta_{x_0}) \tag{49}$$

where

$$J=\int_0^{x_{\max}}\left[t+d\cdot\left(1-\frac{x_{\max}}{x}\cdot K\right)\right]^2\Big/\left[d^3\cdot\left(-\frac{x_{\max}}{x}\cdot K\right)^3\right]Bdx \tag{50}$$

$$B=\left(\ell n\frac{x_0+x_{\max}}{x_0+x}\right)\Big/\left(\ell n\frac{x_0+x_{\max}}{x_0}\right) \tag{51}$$

$$K=\frac{\ell n\dfrac{x_0+x}{x_0}+\sum_{i=1}^{k}(k-i)\ell n\dfrac{x_0+x_i}{x_0+x_{i-1}}}{\ell n\dfrac{x_0+x_{\max}}{x_{\max}}+\sum_{i=1}^{m}(m-i)\ell n\dfrac{x_0+x_i}{x_0+x_{i-1}}} \tag{52}$$

$$K(d)=8/f \tag{53}$$

The numerical value of J is taken as negative.

Equations (44), (45), and (49) incorporate the term $x_0=10^{-2}$ m. It should be considered constant and dependent upon the construction of the experimental evaporator unit. In heat pipes, the groove section occupied with the artery barrier is so small that it can be neglected. Therefore, in calculating evaporators by Eqs. (44), (45), and (49), $x_{\max}$ may be taken equal to the whole groove length and $x_0=10^{-2}$ m may be considered constant.

V. Comparison of the Experimental and Predicted Data

In experiments, we have recorded the heat flux as a function of the groove wall superheat above saturation temperature. The heat flux increases with ΔT_m. At small superheats (5 + 10 K), evaporative heat transfer occurs. The undisturbed fluid flow and its recession into the groove are clearly observed. As superheat increases, nucleation initiates in the fluid flow. Since the vapor pressure in the bubble is higher than the saturation one, the bubble collapses with fluid spraying. The spraying intensity, increasing with superheat, qualitatively estimates heat-transfer rate in the groove. However, the increase in heat removal with growing superheat is not unlimited. At a certain value of ΔT_m, the heat flux achieves its maximum, since the heat power is comparable with the maximum possible heat removal provided by the groove. The higher the test fluid rate in the groove, the greatest amount of power it can transport.

In triangular grooves, the bottom width varies from $0.25\cdot10^{-3}$ to $0.8\cdot10^{-3}$ m, the apex angle from 15 deg to 90 deg, and the evaporator length from $5\cdot10^{-3}$ m to $40\cdot10^{-3}$ m. The experimentally obtained value is:

$$K(\alpha)=0.0535\,(2\alpha)^{1.55} \tag{54}$$

Our investigations have confirmed the assumption on nonuniform heat removal along the groove (Fig. 6). A decrease in the evaporator length $x_{\max}$ from $40\cdot10^{-3}$ m to $5\cdot10^{-3}$ m yields more than a four fold increase of the heat flux, while with uniform heat removal, it should be increased by a factor of 64. It should be noted here that the heat flux in the groove ($x_{\max}=5\cdot10^{-3}$ m) exceeds the predicted critical

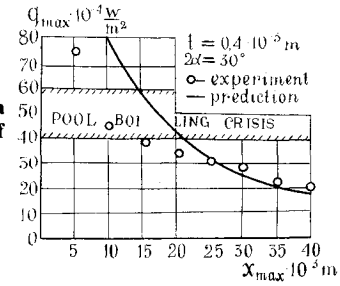

Fig. 6 Maximum heat flux for a triangular groove as a function of the free evaporation surface.

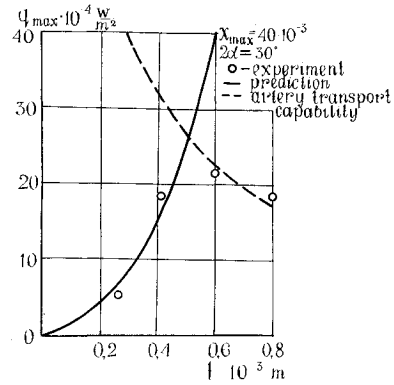

Fig. 7 Maximum heat flux for a triangular groove as a function of the groove width.

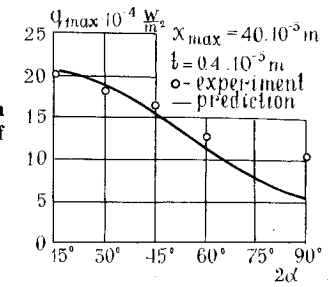

Fig. 8 Maximum heat flux for a triangular groove as a function of the apex angle.

heat flux with pool boiling.[5] This happens because no stable vapor film can be formed as the departure diameter exceeds the groove height. In the subcritical zone, the experimental magnitude of the heat flux is smaller than the predicted value. Probably, increasing nucleation and forming dry spots on the groove wall exert an additional resistance to the test fluid flow.

The growth of the groove width causes increasing fluid flow rate. Consequently, heat transfer is enhanced. However, with increasing groove width, the equivalent radius also becomes greater, but the capillary pressure responsible for fluid motion in the artery decreases (Fig. 7).

The experimental and predicted data for the groove with the apex angle varying from 15 to 90 deg are shown in Fig. 8. With growing angle, the effective groove section diminishes, thereby reducing heat removal. Experimental and predicted values agree well for the angles between 15 and 60 deg. For the 90 deg angle, the experimental value of the heat flux greatly exceeds the predicted one. At larger angles, the capillary pressure decreases sharply, and fluid spraying at boiling exerts the dominating influence on heat transfer.

For rectangular grooves, the experimental coefficient $K(d)$ is equal to:

$$K(d) = 14.5\,(t/2d) \tag{55}$$

The evaporators with the grooves of constant width ($t = 0.4\cdot10^{-3}$ m) and length ($x_{max} = 40\cdot10^{-3}$ m), whose depth ranges from $0.2\cdot10^{-3}$ m to $1.6\cdot10^{-3}$ m have been studied. The increasing depth causes the growth of the effective groove section and enhancement of acetone circulation. However, in a very deep groove, the bubble rise is difficult and hampers fluid flow. This leads to a certain decrease of heat removal in very deep grooves (Fig. 9).

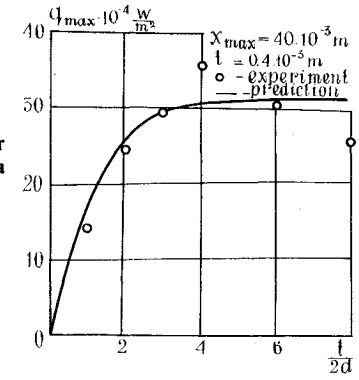

Fig. 9 Maximum heat flux for a rectangular groove as a function of the groove depth.

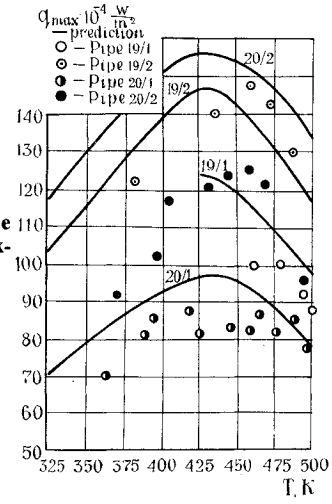

Fig. 10 Comparison of the predicted data with the experimental results of Moritz.

VI. Comparison With Other Data

Comparison of the predictions by Eq. (44) and Moritz' experimental data[1] is shown in Fig. 10. Sufficient agreement (25%) between theory and experiment is observed.

The predicted optimum value ($2\alpha = 38$ deg) of the apex angle for the triangular groove with a constant depth agrees well with Bressler and Wyatt's calculation results.[2]

VII. Conclusions

1) Experiments have been conducted with acetone evaporation and boiling heat transfer in thin-film evaporators with triangular and rectangular grooves with heating under the third-order boundary conditions (new data).

2) Design formulas are derived for maximum heat flux with acetone evaporation and boiling in different configuration grooves under the third-order boundary conditions. The predictions data agree well with the experimental results (new data).

3) The experimental heat flux with acetone boiling in the grooves of thin-film evaporators is shown to exceed the predicted value with acetone pool boiling.

References

[1] Moritz, K., "On the Effects of Capillary Geometry on the Optimal Heating Surface Loads in Heat Pipes," *Heat Pipes*, Izd. Mir, Moscow, 1972, pp. 33-117.

[2] Bressler, R. G. and Wyatt, R. W., "Surface Wetting Through Capillary Grooves," *Journal of Heat Transfer*, Vol. 92, Feb. 1970, pp. 126-132.

[3] Feldman, K. T. and Berger, M. E., "Analysis of a High-Heat Flux Water Heat Pipe Evaporator," Tech. Rept. ME 62(73) ONR-012-12, 1973.

[4] Vasiliev, L. L. and Abramenko, A. N., "Study of Heat and Mass Transfer in Heat Pipe-Based Exchangers," *Proceedings of the Second International Heat Pipe Conference*, Bologna, Italy, 1976, pp. 463-472.

[5] Tong, L. S., *Boiling Heat Transfer and Two-Phase Flow*, John Wiley and Sons, Inc., New York-London-Sydney.